PERGAMON

International Journal of Solids and Structures 37 (2000) 6177–6202

INTERNATIONAL JOURNAL OF SOLIDS and STRUCTURES

www.elsevier.com/locate/ijsolstr

High strain-rate shear-strain localization in f.c.c. crystalline materials: a perturbation analysis

M.A. Zikry*, M.R. Pothier, J.N. Baucom

Department of Mechanical and Aerospace Engineering, North Carolina State University, Raleigh, NC 27695, USA

Received 17 July 1998; in revised form 14 September 1999

Abstract

A new perturbation formulation has been developed that is based on a rate-dependent crystalline plasticity constitutive formulation to investigate planar high strain-rate instabilities and shear-strain localization in face-centered cubic (f.c.c.) crystalline materials. This new formulation can account for strain-rate sensitivity values that range from rate-independent to highly rate-dependent values. Hence, accurate and detailed predictions of material instabilities and shear-strain localization can be obtained for high strain-rate deformations of crystalline materials that are rate-sensitive, such as f.c.c. materials. Critical instability parameters are obtained for deformation modes that account for the effects of strain-rate history, inertia, strain-hardening, wave number, and thermal and geometrical softening for applied strain-rates that range from 100 to 5000 s^{-1}. Post-instability behavior and localization modes are monitored by tracking the rate of growth of stability parameters beyond the initial instability point. Results from these perturbation analyses are in good agreement with rate-independent limiting cases and high strain-rate experimental observations. The present study underscores the importance of characterizing material instabilities and shear-strain localization in terms of the competing softening and hardening mechanisms of the lattice structure.

Keywords: Shear strain localization; High strain-rate; f.c.c. Crystalline materials; Perturbation analyses; Material failure and instability

1. Introduction

The localization of plastic deformation is observed in various applications such as high speed machining, ballistic impacts, and metal forming. Localization, in the sense of a deformation pattern

* Corresponding author. Tel.: +1-919-515-2365; fax: +1-919-515-7968.
E-mail address: zikry@eos.ncsu.edu (M.A. Zikry).

0020-7683/00/$ - see front matter
PII: S0020-7683(99)00266-8

involving one or more intense deformation bands, frequently occurs in a wide variety of solids such as structural metals, polymers, rocks and concrete, and such localizations are generally a precursor to ductile fracture.

Shear-strain localization in various materials can be classified as a function of loading conditions. Shear localization may occur in materials subjected to quasi-static rate-independent isothermal conditions. It can also occur due to material mechanisms associated with dynamic and adiabatic deformations in rate-dependent materials. In materials subjected to quasi-static loading conditions, a shear instability may be viewed as a material instability that occurs due to the loss of ellipticity of the equilibrium equations. Material instabilities of this general classification have been investigated by Hadamard (1903), Thomas (1961), Hill (1962), Mandel (1966) and Rice (1977). Within this framework, for rate-independent solids, a condition governing bifurcation into the localized band is obtained. This bifurcation coincides with the loss of ellipticity of the equations associated with a quasi-static deformation. There is also a correspondence between the condition for a localization bifurcation and the occurrence of stationary waves. Thus, for rate-independent solids, localization can be simultaneously associated with a bifurcation, a change in the type of the governing equations, or the occurrence of stationary body waves. Also within these quasi-static approaches are the bifurcation analyses of Rudnicki and Rice (1975) and Stören and Rice (1975) that have been developed for the flow of granular materials. Instabilities in this case are due to vertex effects arising from the noncoaxiality of the plastic strain-rate tensor with the stress tensor.

A different formulation, within the quasi-static rate-independent approach, for shear localization, is the gradient approach. Here the analytical difficulties associated with the loss of ellipticity are relaxed by assuming a material dependence on the strain and higher order strain gradients. Aifantis (1987) considered hyperelastic materials, for which equilibrium equations lose ellipticity at finite strains, but remain elliptic when high order deformation gradients are considered. Zbib and Aifantis (1988) studied the initiation of shear bands by examining the role of material rotation, strain gradients and strain-rate gradients into the constitutive equation for the flow stress.

At high strain-rates, plastic instabilities are determined by the competition between hardening and softening mechanisms of the material. Generally in rate-dependent materials, phenomenological constitutive formulations for metals remain elliptic and wave speeds are positive. The assumption of global adiabatic deformation is commonly associated with high nominal strain-rates due to the lack of time for heat diffusion, and heat generation is highest in regions of high strain-rates. Shear band formation is dependent on the interrelated mechanisms of thermal softening, heat conduction, inertia, initial inhomogeneities and boundary conditions; see, for example, Rogers (1983).

The stability of solutions of linearized versions of phenomenological thermo-viscoplastic constitutive formulations has been used to investigate shear band evolution in metals. Bai (1981, 1982) considered the dynamic simple shear problem in an analysis similar to a quasi-static analysis employed by Clifton (1980). Ordinary differential equations with constant coefficients were obtained by neglecting the time dependence of the unperturbed homogeneous solution. Fressengeas and Molinari (1985) examined the influence of inertial and thermal effects on ductility for a one-dimensional uniaxial tension model. Anand et al. (1987) used a three-dimensional linear perturbation of shear localization to investigate shear band formation in isotropic, incompressible viscoplastic materials. Molinari and Clifton (1983) and Clifton and Molinari (1988) also obtained critical conditions for shear localization in thermo-viscoplastic materials in closed form for idealized models of simple shear. Heat conduction, inertia, and elasticity were neglected. Wright and Batra (1985) used a perturbation analysis with a finite element analysis to determine the deformation patterns after the point of instability for one-dimensional simple shear for a thermo-viscoplastic material. Wright and Walter (1987) and Wright (1992) also compared the perturbation results with numerical

methods. In the study by Wright (1992) a perturbation analysis was used to investigate the effects of work hardening, strain-rate hardening and thermal softening on the formation of shear bands in simple shear, for a thermo-viscoplastic material. Dudzinski and Molinari (1991) used a perturbation analysis to study thermo-viscoplastic instabilities in biaxial loading. The rate of growth of the instability was characterized in terms of an effective instability analysis. Biaxial stretching was studied by Zhu et al. (1992) using a phenomenological model for a viscoplastic material with isotropic and kinematic hardening. They showed that the backstress, plastic spin and texture development have a significant effect on material instability. They used a perturbation analysis in which one variable was perturbed. Zhu et al. (1995) considered the dynamic aspects of dynamic shear band formation in gradient-dependent thermo-viscoplastic materials subjected to simple shearing. They used a linear stability analysis and a numerical solution of a nonlinear problem to develop solutions that relate shear band length to a deformation length scale that results from strain gradients and a thermal length scale that results from a thermal conductivity parameter. Aifantis (1995) extended this gradient approach to develop solutions for dislocation pattern-forming instabilities related to shear bands and interfaces.

A more physically-based constitutive formulation is one that is based on crystallographic slip. The primary mechanism for inelastic deformation in a single crystal is the movement of dislocations along crystallographic slip planes. Experimental investigations have shown that single f.c.c. crystals undergoing multiple slip often exhibit regions of intense localized shearing. In addition to the softening and hardening mechanisms associated with phenomenological adiabatic high strain-rate formulations, crystalline plasticity constitutive formulations are characterized by the rotation of the lattice, which results in geometrical softening. Geometrical softening results in lattice orientations favorable to the formation of shear bands.

Shear band initiation in rate-independent single crystals subjected to quasi-static loading conditions was investigated by Asaro (1979). He used a bifurcation method with a double slip model to obtain orientations favorable to shear band formation under uniaxial loading conditions. Molinari (1988) used a linear perturbation analysis, similar to the analysis of Dudzinski and Molinari (1991), to study shear band initiation in f.c.c. single crystals. He used an assumption of small limiting values for the rate sensitivity parameter. This approximation resulted in a 3×3 matrix which was used to obtain roots that characterized the onset of instability in a single crystal. Elasticity and thermal and geometrical softening were not included in this analysis.

The major objective in this study is to gain a more detailed and improved understanding of high strain-rate mechanisms associated with adiabatic shear band formation in single f.c.c. crystals. A rate-dependent crystalline constitutive formulation and a linear perturbation analysis of all pertinent variables will be employed to characterize the competition between the softening and hardening mechanisms of the monocrystalline structure, for nominal strain-rates ranging from 100 to 5000 s^{-1}. The effects of strain-rate sensitivity, inertia, strain-rate history, strain hardening, wave number, and thermal and geometrical softening on crystalline shear-strain localization will be investigated. An essential and unique feature of this perturbation analysis is the use of a range of rate sensitivity parameters, physically representative of rate-dependent f.c.c. crystals subjected to high strain-rates. By not assuming small limiting values for the rate sensitivity parameter, perturbation equations are derived that result in improved predictions and a detailed understanding of shear-strain localization in single crystals subjected to high rates of strain. Material instabilities are investigated by perturbing all pertinent variables, and the rate of growth of instabilities, beyond the initial instability point, is monitored to characterize post-instability behavior and localization modes. This rate of growth is used to distinguish material instabilities from shear-strain localization. The present results are verified by comparisons with special limiting cases and experimental observations.

2. Constitutive formulation

In this section, the governing equations and the crystalline constitutive formulation for the high strain rate deformation of rate-dependent single crystals are developed. The constitutive framework for this study is based on the formulation developed by Zikry (1994).

The velocity gradient is decomposed into its symmetric and anti-symmetric parts,

$$V_{i,j} = D_{ij} + W_{ij}, \tag{1}$$

where the deformation rate tensor and spin tensor, respectively, are given by

$$D_{ij} = \frac{1}{2}\left(V_{i,j} + V_{j,i}\right) \tag{2a}$$

and

$$W_{ij} = \frac{1}{2}\left(V_{i,j} - V_{j,i}\right). \tag{2b}$$

The deformation rate and spin tensors are decomposed into elastic and inelastic components,

$$D_{ij} = D^{*}_{ij} + D^{\mathrm{p}}_{ij} \tag{3a}$$

and

$$W_{ij} = W^{*}_{ij} + W^{\mathrm{p}}_{ij}. \tag{3b}$$

The superscript $*$ denotes the elastic part, and the superscript p denotes the plastic part; W^{*}_{ij} includes rigid body spin.

The plastic parts are defined in terms of the crystallographic slip rates as

$$D^{\mathrm{p}}_{ij} = P^{(\alpha)}_{ij}\dot{\gamma}^{(\alpha)} \tag{4a}$$

and

$$W^{\mathrm{p}}_{ij} = \omega^{(\alpha)}_{ij}\dot{\gamma}^{(\alpha)}, \tag{4b}$$

where α is summed over all active slip systems. The tensors $P^{(\alpha)}_{ij}$ and $\omega^{(\alpha)}_{ij}$ are defined as

$$P^{(\alpha)}_{ij} = \frac{1}{2}\left(s^{(\alpha)}_{i}m^{(\alpha)}_{j} + s^{(\alpha)}_{j}m^{(\alpha)}_{i}\right) \tag{5a}$$

and

$$\omega^{(\alpha)}_{ij} = \frac{1}{2}\left(s^{(\alpha)}_{i}m^{(\alpha)}_{j} - s^{(\alpha)}_{j}m^{(\alpha)}_{i}\right), \tag{5b}$$

where $m^{(\alpha)}_{i}$ is the unit normal to the slip plane, and $s^{(\alpha)}_{i}$ is the unit vector in the slip direction.

For a rate-dependent formulation, the resolved shear stresses are functions of the slip-rates,

$$\tau^{(\alpha)} = \tau^{(\alpha)}_{\mathrm{r}}\left(\frac{\dot{\gamma}^{(\alpha)}}{\dot{\gamma}_{\mathrm{r}}}\right)^{m} \quad \text{(no sum on } \alpha\text{)}, \tag{6}$$

where $\dot{\gamma}_r$ is a reference shear-strain rate corresponding to a reference shear stress on the αth slip system. Based on the work of Zikry (1994), the following reference stress is used to account for strain hardening and thermal softening:

$$\tau_r^{(\alpha)} = \tau_y^{(\alpha)} \left(\frac{\gamma}{\gamma_r} + 1 \right)^n \left(\frac{T}{T_r} \right)^{-\nu}, \tag{7}$$

where n is a strain hardening parameter exponent, ν is a thermal softening exponent, γ_r is a reference shear-strain, and T_r is a reference temperature. The rate sensitivity parameter, m, is material dependent and has important implications in high strain-rate analyses. For values of the slip-rate smaller than a critical value, the lattice is thermally activated; see Follansbee et al. (1984). For slip rates greater than the critical slip rate, the flow is characterized by drag-controlled dislocation motion, and the rate sensitivity parameter is approximately equal to one. The rate independent limit is approached as the rate sensitivity parameter approaches zero, and the resolved shear stress, $\tau^{(\alpha)}$, on slip system α is given in terms of the Cauchy stress, σ_{ij},

$$\tau^{(\alpha)} = P_{ij}^{(\alpha)} \sigma_{ij}. \tag{8}$$

The equations of motion are given by

$$\sigma_{ji,\,j} = \rho \dot{V}_i, \tag{9}$$

where ρ is the material density and the superimposed dot denotes differentiation with respect to time.

Due to the high strain rates used in this analysis, heat conduction is neglected and the process is considered adiabatic; see, for example, Culver (1973). Using a thermodynamic balance of energy, the heat equation is

$$\dot{T} = \frac{\chi}{\rho c_p} D_{ij}^p \sigma_{ij}. \tag{10}$$

In this equation, χ is the fraction of plastic work converted to heat, and c_p is the specific heat of the material.

3. Perturbation analysis

3.1. Perturbation method

The stability of the homogeneous solution is analyzed by adding a small perturbation to the basic solution at a time specified by t_0. The growth or decay of this perturbation characterizes the stability of the solution; growth is an indication of material instability. The form of the perturbed solution, S_i, is given by

$$S_i = S_i^0 + \delta S_i, \tag{11}$$

where the superscript 0 denotes the homogeneous solution (zeroth-order term), and δS_i is the perturbation (first-order term). For δS_i, we use a perturbation of the form

$$\delta S_i = \varepsilon S_i^* \, e^{\eta(t - t_0)} \cos\left(\xi n_j x_j\right), \tag{12}$$

which is used for all variables except the velocity components for which we use

$$\delta V_i = \varepsilon V_i^* \, e^{\eta(t-t_0)} \sin(\xi n_j x_j). \tag{13}$$

The expansion is uniformly valid throughout the domain of the independent variables, η, ξ, t, n_i, and x_i, and is therefore a *regular* perturbation. This perturbed expression is one that has been used by several investigators; see, for example, Clifton et al. (1984), Molinari (1988) and Zhu et al. (1992). In Eqs. (12) and (13), the real part of η characterizes the growth or decay of the perturbation, ε is a small linearization parameter, and ξ, the wave number, characterizes the spatial modulation of the magnitude of the perturbation. As shown in Fig. 1, the value of θ determines the orientation of the shear band with respect to the stress axis.

The homogeneous system of equations is perturbed using Eqs. (11)–(13). The zeroth-and first-order terms are retained in the expansion. The higher order terms in this regular perturbation are neglected because ε may be taken arbitrarily small. The zeroth-order terms correspond to the homogeneous solution, and the first-order terms result in a linearized system of equations of the form

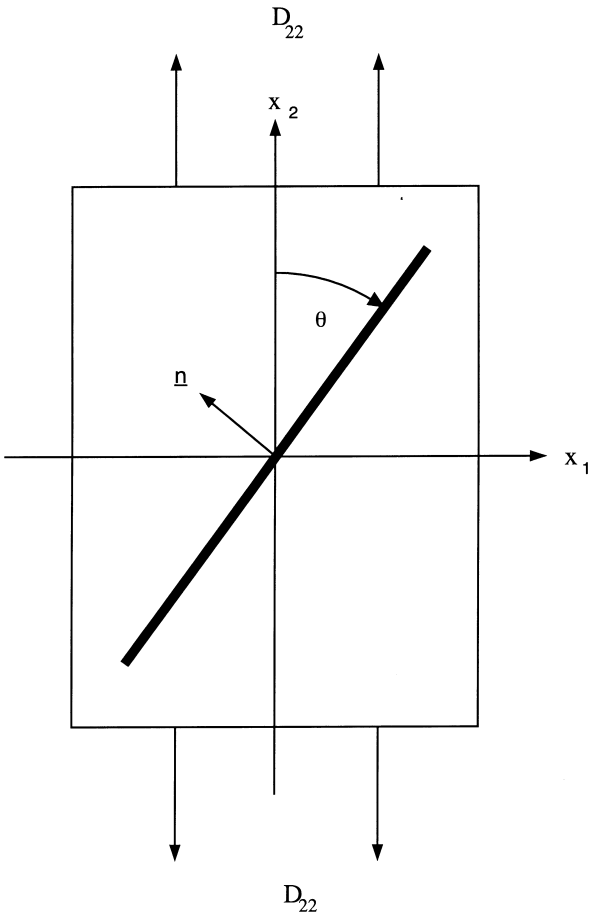

Fig. 1. Orientation of shear band and slip systems.

$$A_{ij}S_j^* = 0, \tag{14}$$

where A_{ij} is the coefficient matrix and S_j^* is a function of the homogeneous solution and of the parameters, η, ξ, and θ. Non-trivial solutions of Eq. (14) exist only if

$$\det(A_{ij}) = 0. \tag{15}$$

Eq. (15) is solved for η, whose real part is used to characterize stability as a function of specified deformation variables.

3.2. Homogeneous solution

The constitutive model for the high strain rate deformation of the single crystal and the proposed perturbation analysis are used to investigate the planar problem of uniaxial strain. Since the modes of deformation considered in this study are planar, we use a resultant double-slip model, similar to the model used by Zikry (1994). Furthermore, inelastic strains are usually much larger than the elastic strains, so elasticity has been neglected in this study; see, for example, Wright (1992). The inelastic deformation is also assumed to be incompressible.

For the uniaxial strain problem, a velocity is imposed in the x_2 direction resulting in an axial strain-rate. For the double slip mode of deformation, we designate one slip system as slip system number one and the other slip system as slip system number two, as shown in Fig. 1. The angle between the slip systems is given by 2ϕ, and ψ is the angle between the slip direction of slip system one and the stress axis. The slip unit vectors and normal unit vectors are

$$\underline{s}^{(1)} = \begin{Bmatrix} \sin\psi \\ \cos\psi \\ 0 \end{Bmatrix}, \tag{16a}$$

$$\underline{m}^{(1)} = \begin{Bmatrix} -\cos\psi \\ \sin\psi \\ 0 \end{Bmatrix}, \tag{16b}$$

$$\underline{s}^{(2)} = \begin{Bmatrix} -\sin(2\phi-\psi) \\ \cos(2\phi-\psi) \\ 0 \end{Bmatrix}, \tag{16c}$$

$$\underline{m}^{(2)} = \begin{Bmatrix} \cos(2\phi-\psi) \\ \sin(2\phi-\psi) \\ 0 \end{Bmatrix}. \tag{16d}$$

The components of the deformation rate tensor are obtained from Eqs. (4a) and (16),

$$D_{11} = -\frac{1}{2}\dot{\gamma}^{(1)}\sin 2\psi - \frac{1}{2}\dot{\gamma}^{(2)}\sin(4\phi - 2\psi), \tag{17}$$

$$D_{22} = \frac{1}{2}\dot{\gamma}^{(1)}\sin 2\psi + \frac{1}{2}\dot{\gamma}^{(2)}\sin(4\phi - 2\psi), \tag{18}$$

$$D_{12} = -\frac{1}{2}\dot{\gamma}^{(1)}\cos 2\psi + \frac{1}{2}\dot{\gamma}^{(2)}\cos(4\phi - 2\psi). \tag{19}$$

The resolved shear stresses are defined using Eqs. (5a), (8), and (16) as

$$\tau^{(1)} = \frac{1}{2}(\sigma_{22} - \sigma_{11})\sin 2\psi - \sigma_{12}\cos 2\psi, \tag{20}$$

$$\tau^{(2)} = \frac{1}{2}(\sigma_{22} - \sigma_{11})\sin(4\phi - 2\psi) + \sigma_{12}\cos(4\phi - 2\psi). \tag{21}$$

The slip rate on the second slip system is found in terms of the slip rate on the first slip system using Eq. (19). For the homogeneous deformation, $D_{12} = 0$, which results in

$$\dot{\gamma}^{(2)} = \frac{\cos 2\psi}{\cos(4\phi - 2\psi)}\dot{\gamma}^{(1)}. \tag{22}$$

Eqs. (18) and (22) can then be used to obtain $\dot{\gamma}^{(1)}$ in terms of D_{22},

$$\dot{\gamma}^{(1)} = \frac{2D_{22}}{\left[\sin 2\psi + \cos 2\psi \tan(4\phi - 2\psi)\right]}. \tag{23}$$

The rotation of the lattice is governed by the rate of change of ψ. If the slip systems are symmetric with respect to the stress axis, then ψ is equal to ϕ.

Using Eqs. (10), (17) and (18), and neglecting elastic strains, we have

$$\dot{T} = \frac{\chi}{\rho c_p}\frac{(\sigma_{22} - \sigma_{11})}{2}\left[\dot{\gamma}^{(1)}\sin 2\psi + \dot{\gamma}^{(2)}\sin(4\phi - 2\psi)\right]. \tag{24}$$

If there is lattice rotation, then ψ varies and the temperature is found numerically from Eq. (24). However, if ψ is constant, Eq. (24) is integrated to obtain a closed form solution; see Pothier (1994). We can now reduce our system of homogeneous equations to nine equations, based on the assumptions of planar deformation, incompressibility, inelasticity, and duplex slip.

From the incompressibility condition and neglecting elasticity, we have

$$\frac{\partial V_1}{\partial x_1} + \frac{\partial V_2}{\partial x_2} = 0. \tag{25}$$

Using Eqs. (2a) and (17)–(19), we obtain the deformation rate components in terms of the slip rates and the slip system orientations as

$$\frac{\partial V_1}{\partial x_1} = -\frac{1}{2}\dot{\gamma}^{(1)}\sin 2\psi - \frac{1}{2}\dot{\gamma}^{(2)}\sin(4\phi - 2\psi), \tag{26}$$

$$\frac{\partial V_1}{\partial x_2} + \frac{\partial V_2}{\partial x_1} = -\dot{\gamma}^{(1)}\cos 2\psi + \dot{\gamma}^{(2)}\cos(4\phi - 2\psi). \tag{27}$$

The total rate of rotation consists of the plastic rate of rotation and an assumed imposed rate of lattice rotation, $\dot{\psi}$,

$$W_{12} = \dot{\psi} + \frac{1}{2}\left(\dot{\gamma}^{(1)} - \dot{\gamma}^{(2)}\right). \tag{28}$$

Using Eqs. (2b) and (28), we have

$$\frac{\partial V_1}{\partial x_2} - \frac{\partial V_2}{\partial x_1} = 2\dot{\psi} + \left(\dot{\gamma}^{(1)} - \dot{\gamma}^{(2)}\right). \tag{29}$$

In two dimensions, Eq. (9) becomes

$$\sigma_{11,\,1} + \sigma_{12,\,2} = \rho \dot{V}_1, \tag{30}$$

$$\sigma_{12,\,1} + \sigma_{22,\,2} = \rho \dot{V}_2. \tag{31}$$

Eq. (30) is differentiated with respect to the spatial coordinate, x_2, and the Eq. (31) is differentiated with respect to the spatial coordinate, x_1. The difference between the two results is taken, yielding

$$\frac{\partial^2}{\partial x_1 \partial x_2}(\sigma_{22} - \sigma_{11}) + \left(\frac{\partial^2}{\partial x_1^2} - \frac{\partial^2}{\partial x_2^2}\right)\sigma_{12} = \rho\left(\frac{\partial \dot{V}_2}{\partial x_1} - \frac{\partial \dot{V}_1}{\partial x_2}\right). \tag{32}$$

Eq. (10) can be simplified using Eqs. (2a) and (25) to give

$$\rho c_{\mathrm{p}} \dot{T} = \chi\left[\frac{\sigma_{12}}{2}\left(\frac{\partial V_1}{\partial x_2} + \frac{\partial V_2}{\partial x_1}\right) - (\sigma_{22} - \sigma_{11})\frac{\partial V_1}{\partial x_1}\right]. \tag{33}$$

To eliminate the resolved shear stresses, Eqs. (6), (20), and (21) are combined to give

$$\tau_{\mathrm{r}}\left(\frac{\dot{\gamma}^{(1)}}{\dot{\gamma}_{\mathrm{r}}}\right)^m = \frac{1}{2}(\sigma_{22} - \sigma_{11})\sin 2\psi - \sigma_{12}\cos 2\psi, \tag{34}$$

$$\tau_{\mathrm{r}}\left(\frac{\dot{\gamma}^{(2)}}{\dot{\gamma}_{\mathrm{r}}}\right)^m = \frac{1}{2}(\sigma_{22} - \sigma_{11})\sin(4\phi - 2\psi) + \sigma_{12}\cos(4\phi - 2\psi). \tag{35}$$

The system of equations that governs the deformation has now been reduced to nine equations: (7), (25)–(27), (29), and (32)–(35). The nine unknowns for the system of homogeneous equations are $\gamma^{(1)}$, $\gamma^{(2)}$, τ_{r}, $(\sigma_{22}-\sigma_{11})$, σ_{12}, T, V_1, V_2, and ψ.

3.3. Perturbed equations

The following perturbations are now applied to the linear system:

$$\gamma^{(1)} = \gamma^{(1)^0} + \varepsilon\gamma^{(1)^*}\, \mathrm{e}^{\eta(t-t_0)}\cos\left[\xi(n_1 x_1 + n_2 x_2)\right], \tag{36a}$$

$$\gamma^{(2)} = \gamma^{(2)^0} + \varepsilon\gamma^{(2)^*}\, \mathrm{e}^{\eta(t-t_0)}\cos\left[\xi(n_1 x_1 + n_2 x_2)\right], \tag{36b}$$

$$(\sigma_{22} - \sigma_{11}) = (\sigma_{22} - \sigma_{11})^0 + \varepsilon(\sigma_{22} - \sigma_{11})^*\, \mathrm{e}^{\eta(t-t_0)}\cos\left[\xi(n_1 x_1 + n_2 x_2)\right], \tag{36c}$$

$$\sigma_{12} = \sigma_{12}^0 + \varepsilon\sigma_{12}^*\, \mathrm{e}^{\eta(t-t_0)}\cos\left[\xi(n_1 x_1 + n_2 x_2)\right], \tag{36d}$$

$$T = T^0 + \varepsilon T^* \, e^{\eta(t-t_0)} \cos\left[\xi(n_1 x_1 + n_2 x_2)\right], \tag{36e}$$

$$V_1 = V_1^0 + \varepsilon V_1^* \, e^{\eta(t-t_0)} \sin\left[\xi(n_1 x_1 + n_2 x_2)\right], \tag{36f}$$

$$V_2 = V_2^0 + \varepsilon V_2^* \, e^{\eta(t-t_0)} \sin\left[\xi(n_1 x_1 + n_2 x_2)\right], \tag{36g}$$

$$\psi = \psi^0 + \varepsilon \psi^* \, e^{\eta(t-t_0)} \cos\left[\xi(n_1 x_1 + n_2 x_2)\right], \tag{36h}$$

$$\tau_r = \tau_r^0 + \varepsilon \tau_r^* \, e^{\eta(t-t_0)} \cos\left[\xi(n_1 x_1 + n_2 x_2)\right]. \tag{36i}$$

Since we perform a *regular* perturbation, only the zeroth- and first-order terms are retained in the expansion. This results in a linearized system of nine perturbed equations. The derivation of the perturbed form for Eq. (34) will be presented here. For detailed derivations of the remaining perturbed equations, obtained in a similar manner, see Pothier (1994).

The variables are perturbed using Eq. (36). For slip system one, the perturbation of the slip rate, $\dot{\gamma}^{(1)}$, is given by

$$\dot{\gamma}^{(1)} \equiv \frac{\partial}{\partial t}\gamma^{(1)} = \dot{\gamma}^{(1)^0} + \varepsilon\eta\gamma^{(1)^*} \, e^{\eta(t-t_0)} \cos\left[\xi(n_1 x_1 + n_2 x_2)\right]. \tag{37}$$

The trigonometric terms are perturbed using the double-angle formula as

$$\sin 2\psi = \sin 2\psi^0 \cos\left\{2\varepsilon\psi^* \, e^{\eta(t-t_0)} \cos\left[\xi(n_1 x_1 + n_2 x_2)\right]\right\} + \cos 2\psi^0 \sin\left\{2\varepsilon\psi^* \, e^{\eta(t-t_0)} \cos\left[\xi(n_1 x_1 + n_2 x_2)\right]\right\}, \tag{38}$$

and since $\varepsilon \ll 1$, we have

$$\sin 2\psi = \sin 2\psi^0 + 2\varepsilon\psi^* \cos 2\psi^0 \, e^{\eta(t-t_0)} \cos\left[\xi(n_1 x_1 + n_2 x_2)\right]. \tag{39}$$

Similarly,

$$\cos 2\psi = \cos 2\psi^0 - 2\varepsilon\psi^* \sin 2\psi^0 \, e^{\eta(t-t_0)} \cos\left[\xi(n_1 x_1 + n_2 x_2)\right]. \tag{40}$$

Using a binomial expansion, and retaining only the first-order terms,

$$\begin{aligned}\left(\dot{\gamma}^{(1)}\right)^m &= \left\{\dot{\gamma}^{(1)^0} + \varepsilon\eta\gamma^{(1)^*} \, e^{\eta(t-t_0)} \cos\left[\xi(n_1 x_1 + n_2 x_2)\right]\right\}^m \\ &= \left(\dot{\gamma}^{(1)^0}\right)^m + m\left(\dot{\gamma}^{(1)^0}\right)^{m-1} \varepsilon\eta\gamma^{(1)^*} \, e^{\eta(t-t_0)} \cos\left[\xi(n_1 x_1 + n_2 x_2)\right].\end{aligned} \tag{41}$$

The above perturbations are substituted into Eq. (34), resulting in

$$\left\{\tau_{\mathrm{r}}^{0}+\varepsilon\tau_{\mathrm{r}}^{0}\,\mathrm{e}^{\eta(t-t_0)}\cos\left[\xi(n_1x_1+n_2x_2)\right]\right\}\cdot\frac{\left\{\left(\dot{\gamma}^{(1)^0}\right)^{m}+m\left(\dot{\gamma}^{(1)^0}\right)^{m-1}\varepsilon\eta\gamma^{(1)^*}\,\mathrm{e}^{\eta(t-t_0)}\cos\left[\xi(n_1x_1+n_2x_2)\right]\right\}}{\left(\dot{\gamma}_{\mathrm{r}}\right)^{m}}$$
$$=\frac{1}{2}\left\{(\sigma_{22}-\sigma_{11})^{0}+\varepsilon(\sigma_{22}-\sigma_{11})^{*}\,\mathrm{e}^{\eta(t-t_0)}\cos\left[\xi(n_1x_1+n_2x_2)\right]\right\}\cdot\left\{\sin 2\psi^{0}+2\varepsilon\psi^{*}\cos 2\psi^{0}\,\mathrm{e}^{\eta(t-t_0)}\cos\left[\xi(n_1x_1+n_2x_2)\right]\right\}-\left\{\sigma_{12}^{0}+\varepsilon\sigma_{12}^{*}\,\mathrm{e}^{\eta(t-t_0)}\cos\left[\xi(n_1x_1+n_2x_2)\right]\right\}^{*}\times\left\{\cos 2\psi^{0}-2\varepsilon\psi^{*}\sin 2\psi^{0}\,\mathrm{e}^{\eta(t-t_0)}\cos\left[\xi(n_1x_1+n_2x_2)\right]\right\}. \tag{42}$$

Expanding, neglecting higher order terms, using

$$\tau_{r}^{0}\left(\frac{\dot{\gamma}^{(1)^0}}{\dot{\gamma}_{\mathrm{r}}}\right)^{m}=\frac{1}{2}(\sigma_{22}-\sigma_{11})^{0}\sin 2\psi^{0}-\sigma_{12}^{0}\cos 2\psi^{0}, \tag{43}$$

and dividing by $\varepsilon\,\mathrm{e}^{\eta(t-t_0)}\cos[\xi(n_1x_1+n_2x_2)]$ results in the perturbed form of Eq. (34):

$$\frac{\tau_{\mathrm{r}}^{0}m\left(\dot{\gamma}^{(1)^0}\right)^{m-1}\eta\gamma^{(1)^*}+\left(\dot{\gamma}^{(1)^0}\right)^{m}\tau_{r}^{*}}{\left(\dot{\gamma}_{\mathrm{r}}\right)^{m}}=\frac{1}{2}\left[2(\sigma_{22}-\sigma_{11})^{0}\psi^{*}\cos 2\psi^{0}+(\sigma_{22}-\sigma_{11})^{*}\sin 2\psi^{0}\right]+2\left[\sigma_{12}^{0}\sin\left(2\psi^{0}\right)\psi^{*}-\cos\left(2\psi^{0}\right)\sigma_{12}^{*}\right]. \tag{44}$$

The remaining eight perturbed equations were derived in a similar manner. The perturbed forms of the nine governing equations are summarized below.

$$\frac{\tau_{\mathrm{r}}^{0}\eta m\left(\dot{\gamma}^{(1)^0}\right)^{m-1}}{\left(\dot{\gamma}_{\mathrm{r}}\right)^{m}}\gamma^{(1)^*}+\left(\frac{\dot{\gamma}^{(1)^0}}{\dot{\gamma}_{\mathrm{r}}}\right)^{m}\tau_{\mathrm{r}}^{*}-\frac{1}{2}\sin\left(2\psi^{0}\right)(\sigma_{22}-\sigma_{11})^{*}+\cos\left(2\psi^{0}\right)\sigma_{12}^{*}-\left[(\sigma_{22}-\sigma_{11})^{0}\cos 2\psi^{0}+2\sigma_{12}^{0}\sin 2\psi^{0}\right]\psi^{*}=0, \tag{45}$$

$$\frac{\tau_{\mathrm{r}}^{0}\eta m\left(\dot{\gamma}^{(2)^0}\right)^{m-1}}{\left(\dot{\gamma}_{\mathrm{r}}\right)^{m}}\gamma^{(2)^*}+\left(\frac{\dot{\gamma}^{(2)^0}}{\dot{\gamma}_{\mathrm{r}}}\right)\tau_{\mathrm{r}}^{*}-\frac{1}{2}\sin\left(4\phi-2\psi^{0}\right)(\sigma_{22}-\sigma_{11})^{*}-\cos\left(4\phi-2\psi^{0}\right)\sigma_{12}^{*}+\left[(\sigma_{22}-\sigma_{11})^{0}\cos\left(4\phi-2\psi^{0}\right)-2\sigma_{12}^{0}\sin\left(4\phi-2\psi^{0}\right)\right]\psi^{*}=0, \tag{46}$$

$$\frac{\sigma_{\mathrm{y}}n}{\gamma_{\mathrm{r}}}\left(\frac{T^{0}}{T_{\mathrm{r}}}\right)^{-\nu}\left(\frac{\gamma^{(1)^0}+\gamma^{(2)^0}}{\gamma_{\mathrm{r}}}+1\right)^{n-1}\gamma^{(1)^*}+\frac{\sigma_{\mathrm{y}}n}{\gamma_{\mathrm{r}}}\left(\frac{T^{0}}{T_{\mathrm{r}}}\right)^{-\nu}\left(\frac{\gamma^{(1)^0}+\gamma^{(2)^0}}{\gamma_{\mathrm{r}}}+1\right)^{n-1}\gamma^{(2)^*}-\tau_{\mathrm{r}}^{*}-\frac{\sigma_{\mathrm{y}}\nu}{T^{0}}\left(\frac{T^{0}}{T_{\mathrm{r}}}\right)^{-\nu-1}\left(\frac{\gamma^{(1)^0}+\gamma^{(2)^0}}{\gamma_{\mathrm{r}}}+1\right)^{n}T^{*}=0, \tag{47}$$

$$-\frac{\partial V_1^0}{\partial x_1}(\sigma_{22}-\sigma_{11})^*+\frac{1}{2}\left(\frac{\partial V_1^0}{\partial x_2}+\frac{\partial V_2^0}{\partial x_1}\right)\sigma_{12}^*-\eta\frac{\rho c_p}{\chi}T^* + \left[\frac{1}{2}\sigma_{12}^0\xi n_2-(\sigma_{22}-\sigma_{11})^0\xi n_1\right]V_1^*+\frac{1}{2}\sigma_{12}^0\xi n_1 V_2^*=0, \tag{48}$$

$$\eta\gamma^{(1)^*}-\eta\gamma^{(2)^*}-\xi n_2 V_1^*+\xi n_1 V_2^*+2\eta\psi^*=0, \tag{49}$$

$$n_1 n_2\xi^2(\sigma_{22}-\sigma_{11})^*+\left(n_1^2-n_2^2\right)\xi^2\sigma_{12}^*-\rho\eta n_2\xi V_1^*+\rho\eta n_1\xi V_2^*=0, \tag{50}$$

$$\eta\sin\left(2\psi^0\right)\gamma^{(1)^*}+\eta\sin\left(4\phi-2\psi^0\right)\gamma^{(2)^*}+2n_1\xi V_1^*+2\left[\dot\gamma^{(1)^0}\cos 2\psi^0-\dot\gamma^{(2)^0}\cos\left(4\phi-2\psi^0\right)\right]\psi^*=0, \tag{51}$$

$$\eta\cos\left(2\psi^0\right)\gamma^{(1)^*}-\eta\cos\left(4\phi-2\psi^0\right)\gamma^{(2)^*}+n_2\xi V_1^*+n_1\xi V_2^* - 2\left[\dot\gamma^{(1)^0}\sin 2\psi^0-\dot\gamma^{(2)^0}\sin\left(4\phi-2\psi^0\right)\right]\psi^*=0, \tag{52}$$

$$n_1\xi V_1^*+n_2\xi V_2^*=0. \tag{53}$$

The nine perturbed equations may be written in matrix form as

$$\begin{bmatrix} A_{11} & 0 & A_{13} & A_{14} & A_{15} & 0 & 0 & 0 & A_{19}\\ 0 & A_{22} & A_{23} & A_{24} & A_{25} & 0 & 0 & 0 & A_{29}\\ A_{31} & A_{31} & -1 & 0 & 0 & A_{36} & 0 & 0 & 0\\ 0 & 0 & 0 & A_{44} & A_{45} & A_{46} & A_{47} & A_{48} & 0\\ \eta & -\eta & 0 & 0 & 0 & 0 & -n_2\xi & n_1\xi & 2\eta\\ 0 & 0 & 0 & n_1 n_2\xi^2 & A_{65} & 0 & -\rho\eta n_2\xi & \rho\eta n_1\xi & 0\\ A_{71} & A_{72} & 0 & 0 & 0 & 0 & 2n_1\xi & 0 & A_{79}\\ A_{81} & A_{82} & 0 & 0 & 0 & 0 & n_2\xi & n_1\xi & A_{89}\\ 0 & 0 & 0 & 0 & 0 & 0 & n_1\xi & n_2\xi & 0 \end{bmatrix}\begin{bmatrix} \gamma^{(1)^*}\\ \gamma^{(2)^*}\\ \tau_r^*\\ (\sigma_{22}-\sigma_{11})^*\\ \sigma_{12}^*\\ T^*\\ V_1^*\\ V_2^*\\ \psi^* \end{bmatrix}=\underline{0} \tag{54}$$

where $\underline{0}$ represents the zero vector. The nonzero coefficients are listed in Appendix A.

3.4. Solution method

A non-trivial solution of the linearized system, Eq. (54), exists only if the determinant of the coefficient matrix is zero. The determinant of the 9×9 matrix can be expanded to obtain the characteristic equation,

$$a_3\eta^3+a_2\eta^2+a_1\eta+a_0=0. \tag{55}$$

Making no rate-independent approximations for the rate sensitivity parameter and fully accounting for inertial and thermal effects, we can obtain all possible roots of the characteristic equation.

The coefficients of η are functions of c_p, m, n, T^0, T_r, $\partial V_1^0/\partial x_1$, $\partial V_1^0/\partial x_2$, $\partial V_2^0/\partial x_1$, χ, ϕ, γ, γ_r, $\dot\gamma^{(\alpha)^0}$, $\dot\gamma_r$, ν, θ, ρ, τ_y, $(\sigma_{22}-\sigma_{11})^0$, σ_{12}^0, τ_r^0, ξ, and ψ^0. The three roots of η are determined analytically. Once the material parameters and loading conditions are specified for each case, the terms associated with each

coefficient are reduced. The stability parameter, η, is then obtained as a time dependent function of a specified deformation variable, such as the accumulated plastic shear-strain, γ, or the shear band orientation, θ. We have derived algebraic expressions for the three roots using the program Mathematica (Wolfram, 1991). With the polynomial in these general terms, we avoid evaluating the matrix for each case. This general formulation enables detailed parametric studies for the evolution of η as a function of various deformation variables.

The condition for instability and possible shear-strain localization is determined based on two criteria. The first criterion is based on choosing the real component of one root of η that first becomes positive as a function of an independent variable, such as γ or θ. We use a modified L_∞ norm to choose the real component of η that first becomes positive,

$$\max \mathrm{Re}\{(\eta_1, \eta_2, \eta_3)\} > 0. \tag{56}$$

The second criterion is based on choosing the value of η corresponding to the highest *rate* of growth of the perturbation beyond the point of instability. As noted by several investigators, the instability point may not uniquely characterize the localization mode that may eventually dominate beyond instability as given by Eq. (56); see, for example, Shawki and Clifton (1989) and Wright (1992). Another localization mode may have a higher rate of growth than the mode that initially delineates the instability point. Therefore, we track all three values of η as functions of a specified independent variable, to measure the intensity of the deformation mode beyond the instability point. As the results will show, the instability point does not always correspond to the fastest growing mode beyond the initial point of instability. Our analysis is based on choosing one of the roots of η that is *both* positive and that also has a higher magnitude, relative to the other values of η.

4. Results and discussion

The constitutive model for the high strain-rate deformation of a single rate-dependent f.c.c. crystal and the perturbation method are applied to study the effects of strain-rate history, material rate sensitivity, wave number, strain hardening, stress axis misalignment, lattice rotation, and thermal softening on material instability and localization. For the planar deformation considered in this investigation, a duplex slip system was used. The stable stress axis direction of $[\bar{1}\ 1\ 2]$ is used here, and hence the active slip systems are $(1\ 1\ 1)[\bar{1}\ 0\ 1]$ and $(\bar{1}\ \bar{1}\ 1)[0\ 1\ 1]$. For the planar model considered in this study, these slip systems are projected onto the $(1\ \bar{1}\ 0)$ plane. The slip systems are initially symmetric with respect to the stress axis. Therefore, the angle, ψ, is initially 35°; see Fig. 1. A velocity is applied in the x_2 direction, which results in an axial nominal strain-rate.

The material properties chosen in this study are representative of single pure copper crystals. The density, ρ, is 8900 kg/m^3, the specific heat, c_p, is 385 J/kg K, the fraction of plastic work converted to heat, χ, is 0.9, and the yield stress, τ_y, is 110 MPa. The reference shear rate, $\dot{\gamma}_r$, in the power law expression, Eq. (6), is 0.001 s^{-1}. The value of reference shear, γ_r, in the reference stress, given by Eq. (7), is 0.01 and the reference temperature, T_r, is 20°C. These values are chosen based on values used by Zikry (1994) for an investigation of high strain-rate void collapse in a single copper crystal.

4.1. Quasi-static deformation

To validate our constitutive and perturbation formulations, we analyzed the limiting case of the quasi static and rate-independent, uniaxial deformation of a single crystal, and we then compared our solution with the bifurcation solution of Asaro (1979). Comparisons were made by two methods. In the first

method, η is expanded asymptotically as a function of m, resulting in a 3×3 system of equations. In the second method, the full 9×9 matrix is employed with a value of m that is representative of rate independent values for single f.c.c. crystals.

As noted earlier, the rate-independent limit is achieved as m approaches zero. Based on this approximation, the stability parameter, η, is expanded asymptotically as a function of m,

$$\eta = \frac{1}{m}\big[\eta_0 + o(m)\big], \tag{57}$$

where m is taken to be infinitesimally small. The reference stress is defined by

$$\dot{\tau}_{\mathrm{r}} = h\Big(\dot{\gamma}^{(1)} + \dot{\gamma}^{(2)}\Big), \tag{58}$$

where h is the hardening parameter and Taylor hardening is assumed (i.e., each slip system hardens at the same rate). Furthermore, inertial, thermal and geometrical softening effects are neglected.

Eqs. (57) and (58) are then used in the perturbed equations, Eqs. (45)–(53), and m is set to zero. This results in a 3×3 system of perturbed equations. Non-trivial solutions exist only if the determinant of the coefficient matrix is zero. Eq. (15) is then solved for η_0, where η_0 is a function of the homogeneous solution, the hardening ratio h/σ and the shear band angle θ. The onset of instability is determined by solving for

$$\eta_0 = 0. \tag{59}$$

Based on Eq. (59), h/σ is obtained as a function of θ. The parameter h/σ represents material hardening. Since σ is an axial tensile stress, the value of h/σ is positive when the material hardens and negative when the material softens.

The results of this perturbation analysis for the limiting case, and a comparison with the results of Asaro (1979) are shown in Fig. 2. There is excellent agreement with the bifurcation analysis. As these results indicate, the critical value of h/σ is 0.038 for both methods, at a shear band angle of 40°. These results indicate that shear bands may form while the material continues to harden.

In the second method, we included the rate sensitivity parameter, m, but used a relatively small value of 0.002 in the full 9×9 matrix, given by Eq. (54). Inertial and thermal effects were still neglected at this point for a comparison with the bifurcation results. Eq. (15) was used to find η as a function of the homogeneous solution, the critical shear band angle θ and h/σ. We checked two shear band orientations, 40° and 45°, at a strain-rate of 100 s^{-1}.

This full perturbation analysis provides further insight into the evolution of the growth parameter as a function of h/σ. For a shear band angle of 40°, the value of h/σ at which the real part of η becomes positive is approximately 0.0345, *nearly identical* to the bifurcation solution (Fig. 3). A shear band orientation of 45° was also used for comparison with the bifurcation solution. The orientation of 45° has special significance, since it corresponds to the orientation of maximum resolved shear stress for a crystal in single slip. The predicted results from the perturbation analysis coincide with the results of the bifurcation analysis. For both methods, the critical value of h/σ is zero for the shear band orientation of 45°.

4.2. Wave number

The wave number, ξ, is related to the inverse of the size of the imperfection. As the wave number, ξ, increases, the size of the imperfection decreases. For the rate-independent, quasi-static case, the results

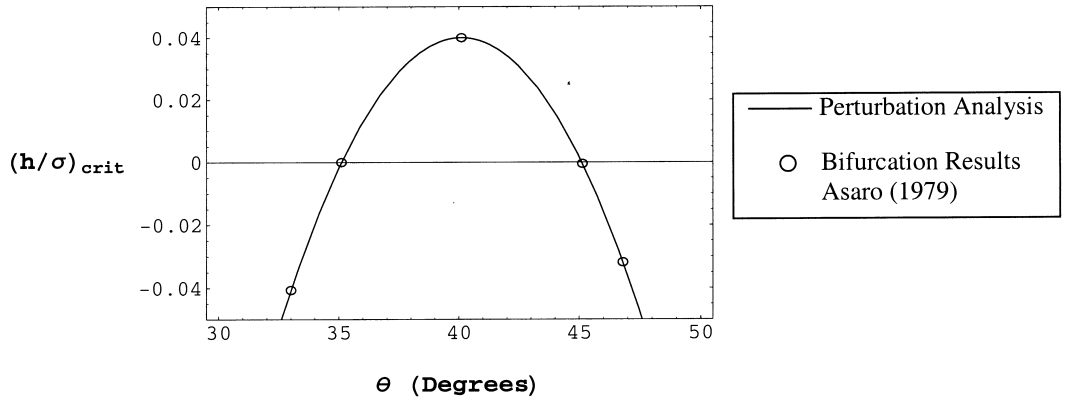

Fig. 2. Critical hardening ratio (h/σ), bifurcation and perturbation analyses.

are independent of the wave number. However, for high strain-rate deformations failure evolution is a function of the wave number and, hence, the size of the imperfection.

We investigated the effects of the wave number on the dynamic deformation of a single crystal at a nominal strain-rate of 100 s^{-1}. We used a thermal softening parameter, ν, of 0.5, a strain hardening parameter, n, of 0.1 and a strain-rate sensitivity, m, of 0.02. Eq. (15) is used to obtain η as a function of ξ for different values of accumulated shear-strain, γ. In this study, the strain at which an instability occurs is denoted as the critical strain. As stated earlier, to measure the strength of the instability, the magnitude of the stability parameter, η, after instability, was also tracked.

As shown in Fig. 4, instabilities are stronger at higher wave numbers. The critical strain decreases as the wave number increases. The critical strains for all wave numbers are between 1.3 and 1.4. The wave number also approaches a limiting value as it is increased. For wave numbers greater than or approximately equal to 200 m^{-1}, the value of η, as a function of wavelength, is essentially constant. Based on the analysis of the variation of η as a function of the wave number, we have used a value of ξ of 200 m^{-1} for all subsequent analyses in this study.

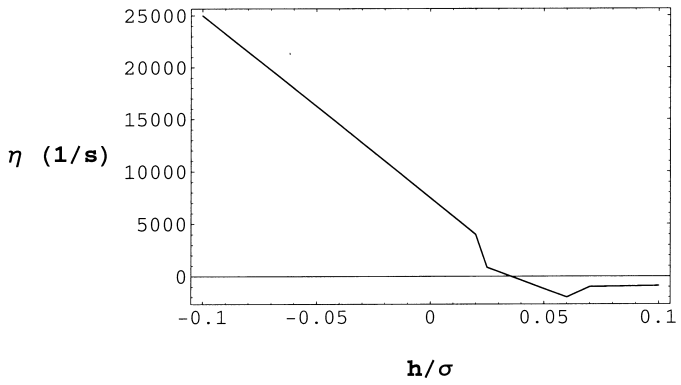

Fig. 3. Stability parameter for a shear band orientation of 40°, rate-independent case.

4.3. Strain-rate history

The effect of strain-rate history on crystal deformation was investigated for nominal strain-rates of 100, 1000, and 5000 s^{-1}. The strain hardening parameter, n, is 0.1, the thermal softening parameter, ν, is 0.5, the shear band angle, θ, is 40°, and the strain-rate sensitivity, m, is 0.02. We obtained η, the growth parameter, as a function of γ, the accumulated plastic strain. The three roots of η for a strain-rate of 5000 s^{-1} are shown in Fig. 5.

As shown in Fig. 6, as the strain-rate increases from 100 to 5000 s^{-1}, the critical strain decreases, and the magnitude of the perturbation growth-rate increases. These critical strains are lower than the critical strain for a nominal strain-rate of 100 s^{-1} (Table 1). This indicates that as the strain-rate increases, initial instabilities will occur at earlier stages of the deformation. Previous experimental results on crystals subjected to high rates of strain indicate that increasing strain-rate promotes localization in single crystals subjected to high strain-rates; see, for example, Marchand and Duffy (1988) and Zikry (1994). This is due to higher rates of unloading at the higher strain-rates.

The stress–strain curve, Fig. 7, also shows the hardening effect of increasing strain-rate. This trend has been shown experimentally; see, for example, Klepaczko and Chiem (1986). However, the maximum resolved shear stress, τ_{max}, for each strain-rate curve occurs at earlier strains as the strain-rate increases, Table 1. The higher strain-rates also had a higher rate of unloading. As noted by Klepaczko and Chiem (1986) this may be due to the increased thermal softening at higher strain-rates due to increasing values of plastic work.

4.4. Strain-rate sensitivity

To investigate the effects of strain-rate sensitivity, we varied the value of the strain-rate sensitivity parameter, m. The shear band angle, θ is taken as 40°, the hardening parameter, n, is 0.1, the thermal softening parameter, ν is 0.5, and the rate sensitivity values are 0.002, 0.01, and 0.02. We investigated these effects for nominal strain-rates of 100 and 1000 s^{-1}.

An increase in strain-rate sensitivity, m, had a stabilizing effect (Fig. 8). An increase in the rate

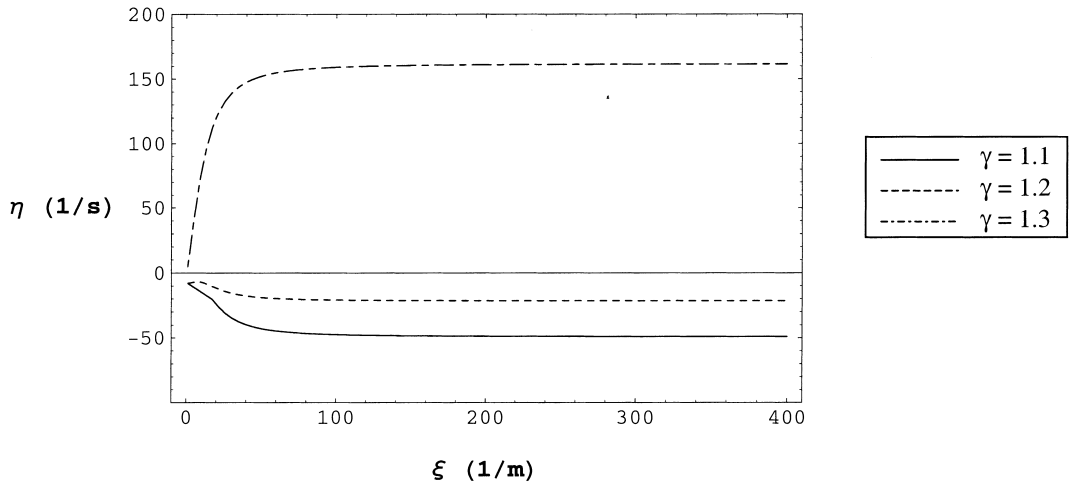

Fig. 4. Stability parameter as a function of wave number for a strain-rate of 100 s^{-1}.

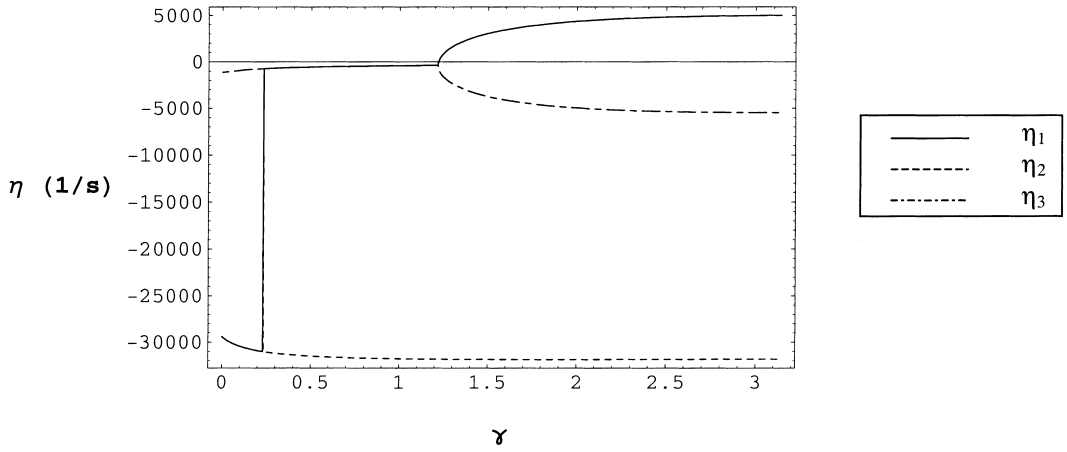

Fig. 5. Roots of η for a nominal strain-rate of 5000 s^{-1}.

sensitivity parameter, m, results in an increase in the critical strain (Table 2). This indicates that an increase in strain-rate sensitivity delays the onset of instabilities that lead to localization. The computational results of Zikry (1994) also support this conclusion. Frantz and Duffy (1972), Follansbee et al. (1984) and Klepaczko and Chiem (1986) also showed experimentally that increasing values of rate sensitivity has a stabilizing effect on deformation, and that increasing the rate sensitivity may delay or preclude the formation of localized patterns in single crystals under high rates of strain.

4.5. Thermal softening

The effects of thermal softening were investigated by varying the thermal softening component, ν, in

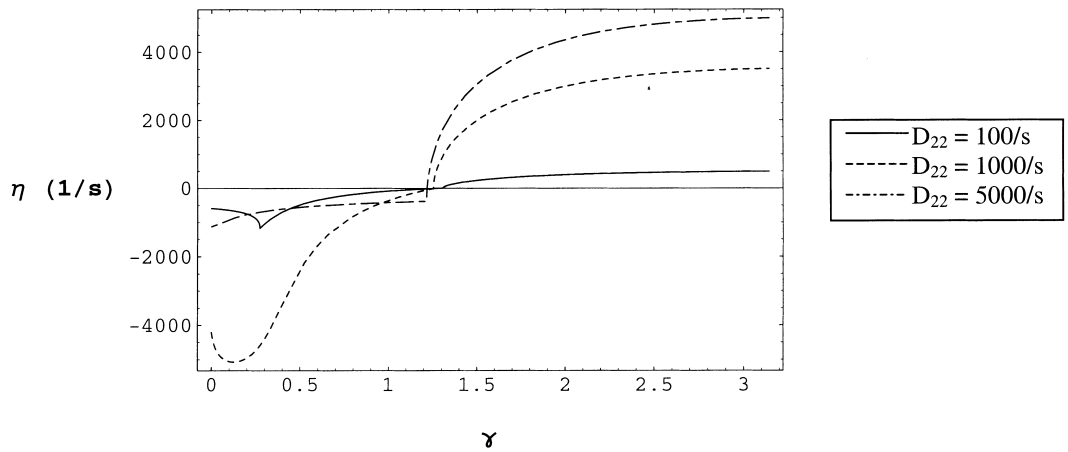

Fig. 6. Strain-rate history effects.

Table 1
Effects of strain-rate history

D_{22} (s^{-1})	γ_{cr}	γ at τ_{max}
100	1.30	1.34
1000	1.25	1.28
5000	1.21	1.24

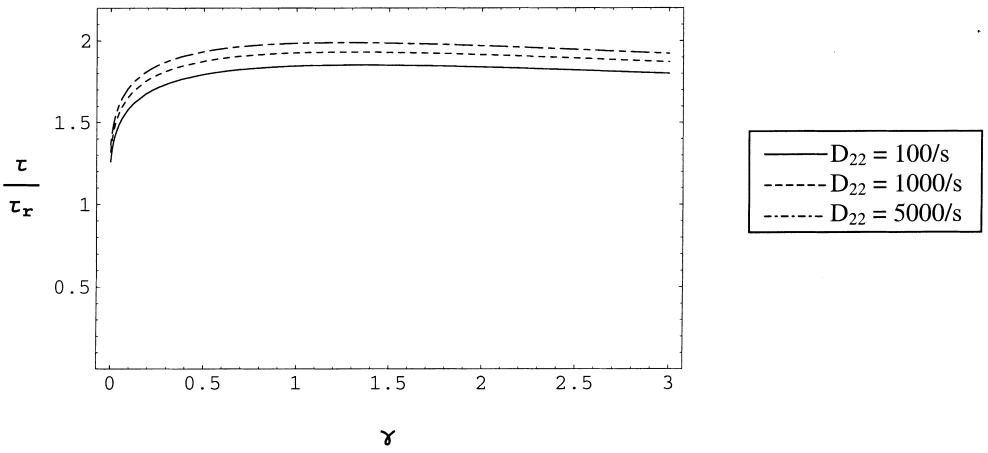

Fig. 7. Stress–strain diagram.

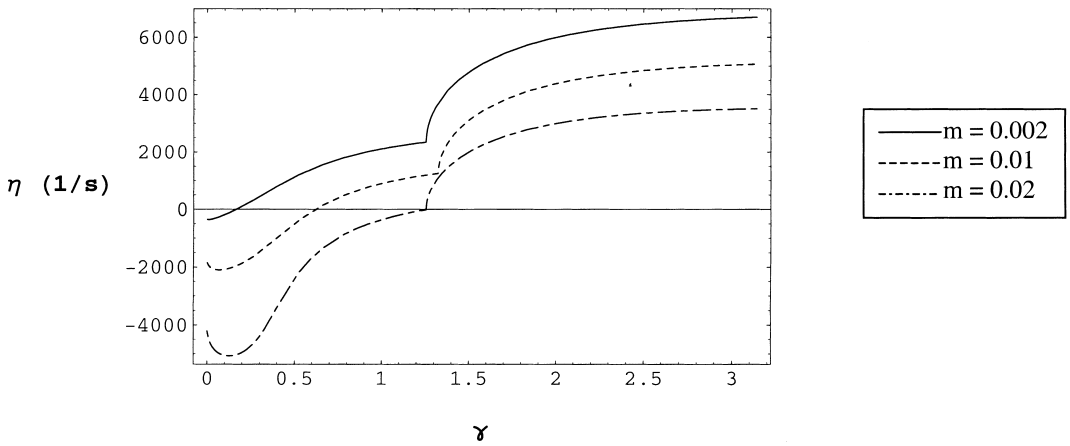

Fig. 8. Strain-rate sensitivity of critical strains for a nominal strain-rate of 1000 s^{-1}.

Table 2
Strain-rate sensitivity of critical strains

Nominal strain-rate (s^{-1})	m	γ_{cr}
100	0.002	0.67
	0.01	0.85
	0.02	1.30
1000	0.002	0.16
	0.01	0.62
	0.02	1.25

the reference stress given by Eq. (7). The temperature independent limit is achieved when ν is zero. For values of ν greater than zero, thermal softening of the flow stress may occur. The values of ν used here are 0.0, 0.3, and 0.5 at a shear band angle, θ of 40°. The strain hardening parameter, n, is 0.1, and the strain-rate sensitivity, m, is 0.02. These effects were investigated for nominal strain-rates of 100 and 1000 s^{-1}.

For both nominal strain-rates, the critical plastic strain decreases as ν increases (Fig. 9). These results underscore the essential role of thermal softening in the formation of adiabatic shear bands. When thermal effects are neglected, instabilities do not occur up to a shear-strain of 300%. However, a slight increase in the thermal softening parameter, ν, results in instabilities occurring at lower critical strains (Table 3). Experimental studies have shown that thermal softening is the dominant mechanism for high strain-rate shear band formation in b.c.c. and f.c.c. crystalline materials; see, for example, Rogers (1979, 1983), Lindholm et al. (1980), Giovanola (1988) and Marchand and Duffy (1988).

4.6. Strain hardening

The effect of strain hardening on material instabilities was investigated by varying the strain hardening parameter n. The values of the strain hardening parameter used are 0.1, 0.2, and 0.5 at a

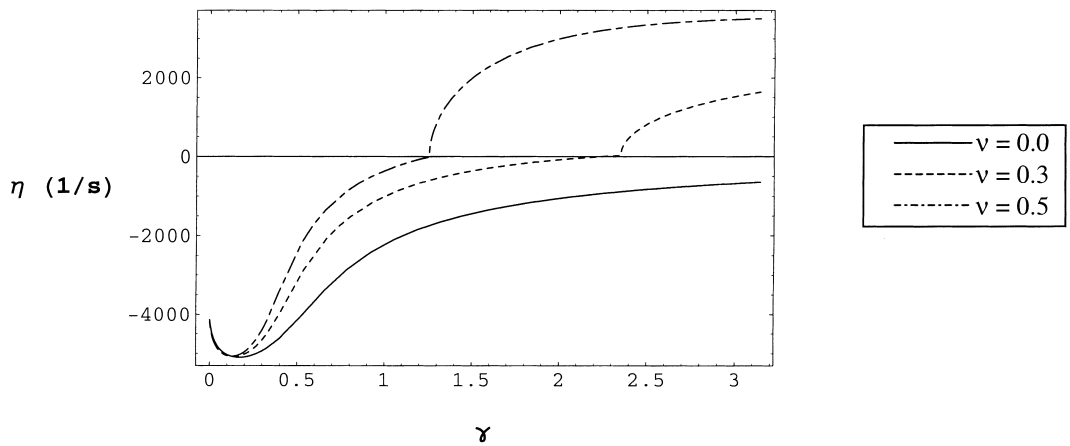

Fig. 9. Thermal effects for a nominal strain-rate of 1000 s^{-1}.

Table 3
Thermal softening effect on critical strains

Nominal strain-rate (s^{-1})	ν	γ_{cr}
100	0.0	3.00+
	0.3	2.33
	0.5	1.30
1000	0.0	3.00+
	0.3	2.25
	0.5	1.25

shear band angle, θ, of 40°. The thermal softening parameter, ν, is 0.5, and the strain-rate sensitivity parameter, m, is 0.02. These effects were investigated for nominal strain-rates of 100 and 1000 s^{-1}.

An increase in the strain hardening parameter, n, results in an increase in the hardening rate of the material. For nominal strain-rates of 100 and 1000 s^{-1}, this has a stabilizing effect on the deformation of the single crystal, Fig. 10. As the strain hardening parameter, n, is increased from 0.1 to 0.2, the point of instability is delayed. When it is increased to 0.5, instabilities do not occur up to a shear-strain of 300%. Critical strains for both nominal strain-rates are given in Table 4. It is well documented that increasing values of strain hardening delay the onset of instability in f.c.c. single crystals subjected to high rates of strain; see, for example, Zikry (1994). This trend has also been shown experimentally by Staker (1981) and Ansart and Dormeval (1988) for steels.

4.7. Asymmetric slip

The effects of asymmetric slip were investigated by two methods. In the first method, each slip system is initially misoriented from the stress axis, resulting in asymmetric slip of the single crystal. This is done to gain further insight into the deformation and localization of single crystals that have initial

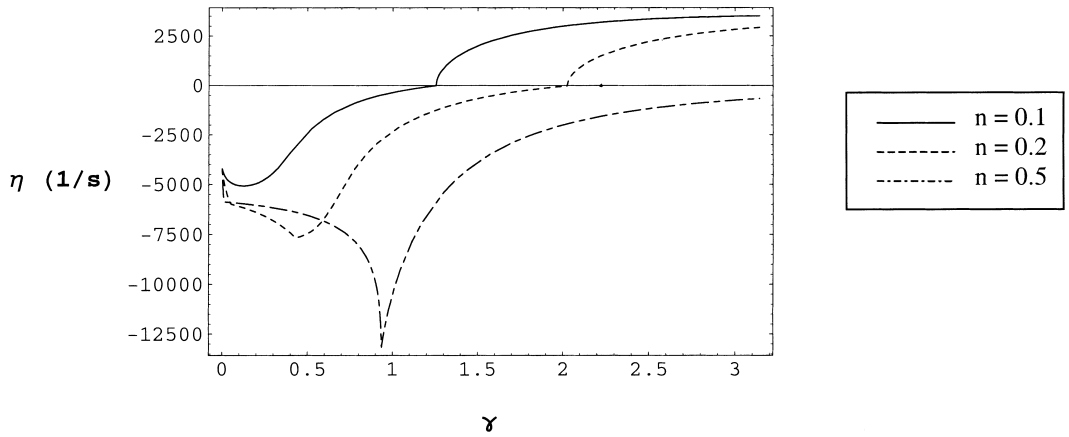

Fig. 10. Strain hardening effects for a nominal strain-rate of 1000 s^{-1}.

misorientations from a stable stress axis. In this method, it is assumed that the orientation is fixed throughout the entire deformation.

In the second method, we investigated the effects of lattice rotation on crystalline deformation and shear-strain localization. In this method, the slip system orientation is updated based on Eq. (28). The resolved shear stresses are no longer constant, and the temperature evolution, given by Eq. (24), must be updated as a function of the rotation, ψ, and the slip rates, $\dot{\gamma}^{(\alpha)}$. The forward Euler method was used to update the temperature.

Critical slip strains were determined for both methods. Furthermore, since the slip systems are not symmetric with respect to the stress axis, it is not reasonable to assume that the initial orientation of the shear band, θ, is 40°. Therefore, for each case, a critical shear band angle is found that corresponds to a relatively strong instability. For both cases, the strain-rate sensitivity, m, is 0.02, the strain hardening parameter, n, is 0.1, and the thermal softening parameter, ν is 0.5, and the nominal strain-rate is 1000 s^{-1}.

4.7.1. Stress axis misalignment

To simulate the effect of an initial misalignment of the stress axis, the slip systems are initially rotated from the stress axis. Referring to Fig. 1, if ψ is chosen greater than the symmetric value of 35°, then, by Eqs. (22) and (23), the primary system is slip system number one and the secondary system is slip system number two. If ψ is chosen less than 35°, then the role of each system is reversed. In this study, we assume clockwise rotation and vary the value of ψ from the initial symmetric orientation of 35° to the maximum resolved shear stress orientation of 45°.

For ψ equal to 35°, the symmetric case, and at shear-strains less than about 1.2, η is negative for all orientations of the shear band, Fig. 11. However, at a shear-strain of 1.3, η is positive at shear band orientations of $\pm$40.8°. The critical strain for this shear band orientation is 1.252. This critical shear band orientation of approximately 40° is a further confirmation that this orientation is reasonable for symmetric duplex slip.

For a one-degree imposed misalignment, the primary slip system is oriented at 36° from the stress axis, and the secondary slip system is oriented at 34° from the stress axis. This preserves the value of 70° between the slip systems. In this case, the critical shear band orientation is 41.6° and the critical slip strain is 1.150. Hence, the shear band is misoriented from the primary slip system by approximately 4°. As noted in experimental studies by Wakefield and Hatherly (1981), Hatherly and Malin (1984), and Harren et al. (1988), this misorientation may be due to secondary slip activity. As the results indicate, there is substantial secondary slip activity, Table 5, that is nearly proportional to the primary slip activity.

The results for fixed clockwise rotations of 0, 1, 2, 5, 8, 9, 9.5, and 10° are summarized in Table 5. In all cases, the shear band is misoriented with respect to the primary slip system. Furthermore, as the

Table 4
Strain hardening effect on critical strains

Nominal strain-rate (s^{-1})	n	γ_{cr}
100	0.1	1.30
	0.2	2.10
	0.5	3.00+
1000	0.1	1.25
	0.2	2.01
	0.5	3.00+

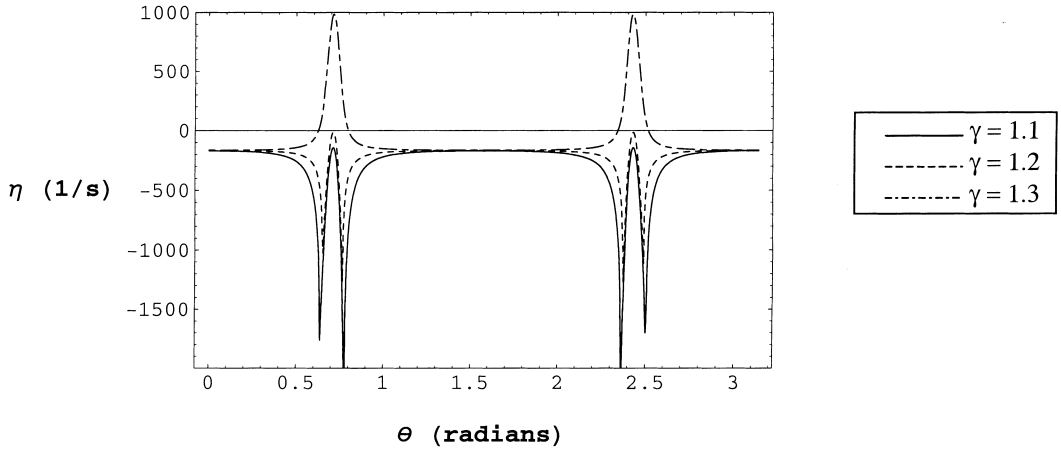

Fig. 11. Perturbation growth-rate as a function of shear band angle for $\psi = 35^\circ$.

stress axis misalignment increases, the secondary slip activity decreases and the angle between the shear band and the primary slip system, $\theta_{cr} - \psi$, decreases.

As indicated in Table 5, as ψ increases, γ_{cr}, decreases. The 5° orientation corresponds to a critical shear band orientation of 45.2°, which is almost coincident with the direction of the maximum resolved shear stress. This decrease in the critical slip strain is most probably due to the critical orientation of the shear band. As noted by Asaro (1979) for the quasi-static deformation of single crystals, and by Zikry (1994) for the high strain-rate analysis of single crystals, shear-strain localization occurs at decreasing strains as the lattice continues to rotate. This decrease in critical strain continues as long as the lattice is misoriented from the shear band, and the shear band orientation is between 35° and 40° from the stress axis. At orientations greater than 40°, the critical strain increases until the primary slip system reaches the plane of maximum shear, when ψ equals 45°. As expected for this case, instabilities occur immediately at the initiation of plastic flow. Similar results are also obtained for a counterclockwise rotation with the shear band forming near the secondary slip system.

4.7.2. Lattice rotation

In the second method, we assume that the slip systems rotate throughout the deformation. The orientation was updated as a function of the rate of lattice spin, given by Eq. (28). In that equation, the imposed rotation is taken as

Table 5
Critical values for clockwise rotation

	Orientation							
	0°	1°	2°	5°	8°	9°	9.5°	10°
$\dot{\gamma}^{(1)}$	1064 s^{-1}	1166 s^{-1}	1266 s^{-1}	1556 s^{-1}	1829 s^{-1}	1916 s^{-1}	1958 s^{-1}	2000 s^{-1}
$\dot{\gamma}^{(2)}$	1064 s^{-1}	961.5 s^{-1}	857.6 s^{-1}	540.3 s^{-1}	217.0 s^{-1}	108.6 s^{-1}	54.30 s^{-1}	0.000 s^{-1}
γ_{cr}	1.252	1.150	1.092	1.050	1.100	1.250	1.280	0.000
θ_{cr}	$\pm 40.8^\circ$	41.6°	42.5°	45.2°	47.6°	48.2°	48.7°	All
$\theta_{cr} - \psi$	5.8°	5.6°	5.5°	5.2°	4.6°	4.2°	4.2°	N/A

Table 6
Critical strains and shear bad angles for lattice rotation

ψ_{init}	ψ_{cr}	θ_{cr}	γ_{cr}	γ_{cr}^{est}	% Difference
35.10°	36.93°	42.4°	1.085	1.092	0.64
35.20°	38.31°	43.6°	1.028	1.040	1.16
35.30°	39.61°	44.8°	1.000	1.011	1.09
35.50°	44.57°	49.2°	1.075	1.074	0.09

$$\psi = \frac{1}{2}\left(\gamma^{(1)} - \gamma^{(2)}\right). \tag{60}$$

The angle of the current slip system orientation is updated by a forward Euler method based on Eq. (60). The temperature evolution, Eq. (24), is also updated in a similar manner, and the stability parameter, η, is obtained as a function of the shear-strain and shear band orientation.

For an initial slip system orientation of 35.1°, the slip systems rotate to 36.93° prior to destabilization. The instability occurs at a critical shear-strain of 1.085 and a critical shear band angle of 42.4°. Similar analyses are performed for initial angles of 35.2, 35.3, and 35.5°. The results, summarized in Table 6, are based on the evolution of the stability parameter, η, as a function of the slip system orientation, ψ, the slip strain, γ, and the shear band orientation, θ.

To compare the results of the two methods of analysis of asymmetric slip, a stability envelope is introduced. The stability envelope is obtained by superimposing the critical strains, obtained from the asymmetric fixed orientation analysis, on a plot of the rotation angle as a function of the accumulated

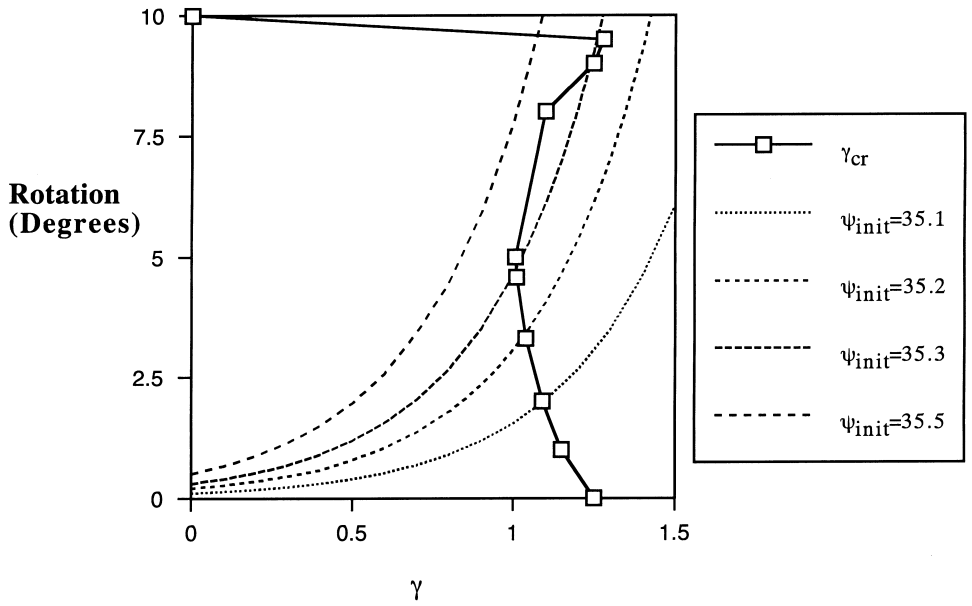

Fig. 12. Predicted critical strains for lattice rotations at a nominal strain-rate of 1000 s^{-1}.

shear-strain, Fig. 12. This provides a method to estimate the critical strains associated with lattice rotation. The critical strain is estimated by determining the strain at which the rotation curve intersects the stability envelope defined by the critical shear-strains obtained from the fixed orientation analysis. The low percent difference between the true critical strains, obtained from the lattice rotation analysis, γ_{cr}, and the estimated critical strains, obtained from the stability envelope, γ_{cr}^{est}, indicates that the stability envelope can accurately identify the critical strains for lattice rotation.

As shown in the stability envelope in Fig. 12, if the initial orientation of the slip systems is nearly symmetric the instability occurs within a small range of shear-strains between 1.0 and 1.3. For initial slip system angles greater than 35.5°, the instability occurs when the primary slip system rotates to 45° from the stress axis. This can occur at shear-strains much less than 1.0 for the larger initial misalignments and indicates that geometrical softening is a dominant localization mechanism when the stress axis is initially misaligned.

5. Conclusions

The thermo-mechanical mechanisms governing material instabilities and shear-strain localization, in f.c.c. crystals subjected to high rates of strain, have been investigated. Rate-dependent crystalline constitutive and new perturbation formulations have been developed and used to characterize failure mechanisms in terms of the competition between the softening and the hardening mechanisms of the crystalline structure. The perturbed system of equations accounts for strain-rate sensitivities that can range from rate-independent to highly rate-dependent values. Stability parameters, which have been obtained as a function of strain-rate sensitivities, strain-rate history, inertia, wave number, and thermal and geometrical softening, have been used to determine domains of material instability. Post-instability behavior and localization modes are characterized by tracking the magnitudes of stability parameters beyond the initial instability point. The present analysis underscores the importance of characterizing the softening and hardening mechanisms associated with the high strain-rate deformation of f.c.c. crystals such that material instabilities and localization modes can be accurately predicted.

Acknowledgements

This work was supported by the National Science Foundation under grant CMS-9713762. This support is gratefully acknowledged.

Appendix A

The following is a list of nonzero components not shown in the coefficient matrix of Eq. (43).

$$A_{11} = \tau_r^0 \eta m \frac{\left(\dot{\gamma}^{(1)^0}\right)^{m-1}}{\left(\dot{\gamma}_r\right)^m}, \quad A_{13} = \left(\frac{\dot{\gamma}^{(1)^0}}{\dot{\gamma}_r}\right)^m, \quad A_{14} = -\frac{1}{2}\sin 2\psi^0,$$

$$A_{15} = \cos 2\psi^0, \quad A_{19} = -(\sigma_{22} - \sigma_{11})^0 \cos 2\psi^0 - 2\sigma_{12}^0 \sin 2\psi^0,$$

$$A_{22} = \frac{\tau_r^0 \eta m \left(\dot{\gamma}^{(2)^0}\right)^{m-1}}{\left(\dot{\gamma}_r\right)^m}, \quad A_{23} = \left(\frac{\dot{\gamma}^{(2)^0}}{\dot{\gamma}_r}\right)^m, \quad A_{24} = -\frac{1}{2}\sin\left(4\phi - 2\psi^0\right),$$

$$A_{25} = -\cos\left(4\phi - 2\psi^0\right), \quad A_{29} = \left(\sigma_{22} - \sigma_{11}\right)^0 \cos\left(4\phi - 2\psi^0\right) - 2\sigma_{12}^0 \sin\left(4\phi - 2\psi^0\right),$$

$$A_{31} = \frac{\sigma_y n}{\gamma_r}\left(\frac{T^0}{T_r}\right)^{-\nu}\left(\frac{\gamma^{(1)^0} + \gamma^{(2)^0}}{\gamma_r} + 1\right)^{n-1}, \quad A_{36} = -\frac{\sigma_y \nu}{T^0}\left(\frac{T^0}{T_r}\right)^{-\nu-1}\left(\frac{\gamma^{(1)^0} + \gamma^{(2)^0}}{\gamma_r} + 1\right)^n,$$

$$A_{44} = -\frac{\partial V_1^0}{\partial x_1}, \quad A_{45} = \frac{1}{2}\left(\frac{\partial V_1^0}{\partial x_2} + \frac{\partial V_2^0}{\partial x_1}\right), \quad A_{46} = -\eta\frac{\rho c_p}{\chi},$$

$$A_{47} = \frac{1}{2}\sigma_{12}^0 \xi n_2 - \left(\sigma_{22} - \sigma_{11}\right)^0 \xi n_1, \quad A_{48} = \frac{1}{2}\sigma_{12}^0 \xi n_1, \quad A_{64} = n_1 n_2 \xi^2,$$

$$A_{65} = \left(n_1^2 - n_2^2\right)\xi^2, \quad A_{67} = -\rho\eta n_2 \xi, \quad A_{68} = \rho\eta n_1 \xi,$$

$$A_{71} = \eta \sin 2\psi^0, \quad A_{72} = \eta \sin\left(4\phi - 2\psi^0\right), \quad A_{77} = 2n_1\xi,$$

$$A_{79} = 2\left[\dot{\gamma}^{(1)^0}\cos 2\psi^0 - \dot{\gamma}^{(2)^0}\cos\left(4\phi - 2\psi^0\right)\right], \quad A_{81} = \eta \cos 2\psi^0,$$

$$A_{82} = -\eta \cos\left(4\phi - 2\psi^0\right), \quad A_{89} = -2\left[\dot{\gamma}^{(1)^0}\sin 2\psi^0 + \dot{\gamma}^{(2)^0}\sin\left(4\phi - 2\psi^0\right)\right].$$

References

Aifantis, E.C., 1987. The physics of plastic deformation. Int. J. Plast 3, 211–247.

Aifantis, E.C., 1995. Pattern formation in plasticity. Int J. Engng 33, 2161–2178.

Anand, L., Kim, K.H., Shawki, T.G., 1987. Onset of shear localization in viscoplastic solids. J. Mech. Phys. Solids 35, 407–429.

Ansart, J.P., Dormeval, R., 1988. Adiabatic shearing in martensitic steels. In: Chiem, C.Y., Kuntze, H.-D., Meyer, L.W. (Eds.), Impact Loading and Dynamic Behavior of Materials Volume 2. DGM Informationsgesellschaft, Germany, pp. 775–782.

Asaro, R.J., 1979. Geometrical effects in the inhomogeneous deformation of ductile single crystals. Acta Metal 27, 445–453.

Bai, Y.L., 1981. A criterion for thermo-plastic shear instability. In: Shock Waves and High Strain-Rate Deformation Phenomena in Metals, Proc. Internat. Conf. on Metallurgical Effects of High Strain-Rate Deformation and Fabrication, Albuquerque, NM. Plenum Press, New York, p. 277.

Bai, Y.L., 1982. Thermo-plastic instability in simple shear. Mech. Phys. Solids 30, 195–207.

Clifton, R.J., 1980. Adiabatic shear banding. In: Materials Response to Ultra-High Loading Rates, NMAB-356. National Advisory Board (NRC), Washington, DC (Chapter 8).

Clifton, R.J., Molinari, A., 1988. Analytical characterization of shear localization in thermo-viscoplastic solids. J. Appl. Mech 54, 806–812.

Clifton, R.J., Duffy, J., Hartley, K.A., Shawki, T.G., 1984. On critical conditions for shear band formation at high strain rates. Scripta Metal 18, 443–448.

Culver, R.S., 1973. Thermal instability strain in dynamic plastic deformation. In: Rohde, R.W., Butcher, B.M., Holland, J.R., Kames, C.H. (Eds.), Metallurgical Effects at High Strain Rates. Plenum Press, New York, pp. 519–530.

Dudzinski, D., Molinari, A., 1991. Perturbation analysis of thermoviscoplastic instabilities in biaxial loading. Int. J. Solids Structures 27, 601–628.

Frantz, R.A., Duffy, J., 1972. The dynamic stress–strain behavior in torsion of 1100-O aluminum subjected to a sharp increase in strain rate. J. Appl. Mech 39, 939–945.

Fressengeas, C., Molinari, A., 1985. Inertia and thermal effects on the localization of plastic flow. Acta Metal 33, 387–396.

Follansbee, P.S., Ragazzoni, G., Kocks, U.F., 1984. The transition to drag-controlled deformation in copper at high strain-rates. In: Mechanical Properties of Materials at High Rates of Strain. Inst. Phys. Conf. Ser., No. 70,71.

Giovanola, J.H., 1988. Adiabatic shear banding under pure shear loading. Part I: Direct observation of strain localization and energy dissipation measurements. J. Mech. Mater 7, 59–71.

Hadamard, J., 1903. Leçons sur la Propagation des Ondes et les Équations de L'Hydrodynamique, Paris.

Hatherly, M., Malin, A.S., 1984. Shear bands in deformed metals. Scripta Metal 18, 449.

Harren, S.V., Dève, H.E., Asaro, R.J., 1988. Shear band formation in plane strain compression. Acta Metal 36, 2435–2480.

Hill, R., 1962. Acceleration waves in solids. J. Mech. Phys. Solids 10, 1–16.

Klepaczko, J.R., Chiem, C.K., 1986. On rate sensitivity of f.c.c. metals, instantaneous rate sensitivity and rate sensitivity of strain hardening. J. Mech. Phys. Solids 34, 29–54.

Lindholm, U.S., Nagy, A., Johnson, G.R., Hoegfeldt, J.M., 1980. Large strain, high strain rate testing of copper. ASME Trans. J. Engrg. Mater. Technol 102, 376–402.

Mandel, J., 1966. Conditions de Stabilité et Postulat de Drucker. In: Kravtchenko, J., Sirieys, P.M. (Eds.), Rheology and Soil Mechanics. Springer–Verlag, Berlin, pp. 58–68.

Marchand, A., Duffy, J., 1988. An experimental study of the formation process of adiabatic shear bands in a structural steel. J. Mech. Phys. Solids 36, 251–283.

Molinari, A., 1988. Shear band analysis. Solid State Phenomena 3/4, 447–468.

Molinari, A., Clifton, R.J., 1983. Localisation de la Déformation Viscoplastique en Cisaillement Simple: Résultats Exacts en Théorie non Linéaire. C.R. l'Acad. Sci. Ser. II 296, 1–4.

Pothier, M.R., 1994. M.Sc. Thesis. North Carolina State University, Raleigh, NC.

Rice, J.R., 1977. The localization of plastic deformation. In: Theoretical and Applied Mechanics, Proc. 14th IUTAM Congress, Delft, The Netherlands. North-Holland, Amsterdam, p. 207.

Rogers, H.C., 1979. Adiabatic plastic deformation. Ann. Rev. Mater. Sci 9, 283.

Rogers, H.C., 1983. Adiabatic shearing — general nature and material aspects in material behavior under high stress and ultrahigh loading rates. In: Mescall, J., Weiss, V. (Eds.), Sagamore Army Research Conference Proceedings 29. Plenum Press, New York, p. 101.

Rudnicki, J.W., Rice, J.R., 1975. Conditions for the localization of deformation in pressure-sensitive dilatant materials. J. Mech. Phys. Solids 23, 371–394.

Shawki, T.G., Clifton, R.J., 1989. Shear band formation in thermal viscoplastic materials. Mechanics of Materials 8, 13–43.

Staker, M.R., 1981. The relation between adiabatic shear instability strain and material properties. Acta Metal 29, 683–689.

Stören, S., Rice, J.R., 1975. Localized necking in thin sheets. J. Mech. Phys. Solids 23, 421–441.

Thomas, T.Y., 1961. Plastic Flow and Fracture in Solids. Academic Press, New York, NY.

Wakefield, P.T., Hatherly, M., 1981. Microstructure and texture of cold-rolled $Cu_{10}Zn$ brass. Met. Sci 15, 109.

Wolfram, S., 1991. Mathematica, A System for Doing Mathematics by Computer. Addison-Wesley, Redwood City, CA.

Wright, T.W., 1992. Shear band susceptibility: work hardening materials. Int. J. of Plasticity 8, 583–602.

Wright, T.W., Batra, R.C., 1985. The initiation and growth of adiabatic shear bands. Int. J. of Plasticity 1, 205–212.

Wright, T.W., Walter, J.W., 1987. On stress collapse in adiabatic shear bands. J. Mech. Phys. Solids 35, 701–720.

Zbib, H.M., Aifantis, E.C., 1988. On the localization and postlocalization behavior of plastic deformation. Part I: On the initiation of shear bands. Int. J. Struct. Mech. Mater. Sci 23, 261.

Zhu, H., Zbib, H.M., Aifantis, E.C., 1992. On the effect of anisotropy and inertia on shear banding: instability of biaxial stretching. Appl. Mech. Rev 45, S110–S117.

Zhu, H., Zbib, H.M., Aifantis, E.C., 1995. On the role of strain gradients in adiabatic shear-banding. Acta Mechanica 111, 111–124.

Zikry, M.A., 1994. Dynamic void collapse and material failure mechanisms in metallic crystals. Mechanics of Materials 17, 273–288.